analytical chemistry

pubs.acs.org/ac Article

Thermal Analysis of a Mixture of Ribosomal Proteins by vT-ESI-MS: Toward a Parallel Approach for Characterizing the *Stabilitome*

Tarick J. El-Baba,[‖] Shannon A. Raab,[‖] Rachel P. Buckley, Christopher J. Brown, Corinne A. Lutomski, Lucas W. Henderson, Daniel W. Woodall, Jiangchuan Shen, Jonathan C. Trinidad, Hengyao Niu, Martin F. Jarrold, David H. Russell, Arthur Laganowsky, and David E. Clemmer*

Cite This: *Anal. Chem.* 2021, 93, 8484−8492 Read Online

ACCESS | Metrics & More | Article Recommendations | Supporting Information

ABSTRACT: The thermal stabilities of endogenous, intact proteins and protein assemblies in complex mixtures were characterized in parallel by means of variable-temperature electrospray ionization coupled to mass spectrometry (vT-ESI-MS). The method is demonstrated by directly measuring the melting transitions of seven proteins from a mixture of proteins derived from ribosomes. A proof-of-concept measurement of a fraction of an *Escherichia coli* lysate is provided to extend this approach to characterize the thermal stability of a proteome. As the solution temperature is increased, proteins and protein complexes undergo structural and organizational transitions; for each species, the folded ↔ unfolded and assembled ↔ disassembled populations are monitored based on changes in vT-ESI-MS charge state distributions and masses. The robustness of the approach illustrates a step toward the proteome-wide characterization of thermal stabilities and structural transitions—the *stabilitome*.

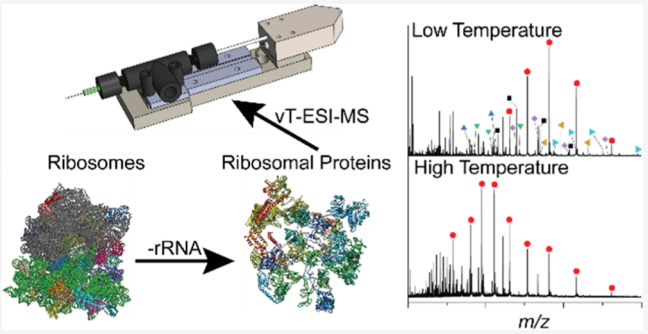

INTRODUCTION

The structures and stabilities of protein conformations are key to maintaining the balance of protein concentrations that are required for proteostasis.[1−4] Most proteins have short biological lifetimes ranging from ∼10 min to 72 h.[5] The lifetime is ultimately defined by the stability of the functional state relative to the denatured state in the environment of the cell. A number of techniques[6−12] have been developed to probe protein thermal stabilities, but the classical method involves monitoring the change in heat *via* calorimetry.[13,14] With commercially available methods, overexpressed and highly purified protein analytes are incrementally heated in a thermally insulated reservoir while monitoring structural changes that occur with the changing temperature.[15] Although protein expression can be scaled to high throughput, measurement of a melting temperature (T_m) using calorimetry or spectroscopy is intrinsically slow, requires a large amount of purified material (0.1−2 mg), and is difficult to multiplex, creating a critical bottleneck for the large-scale evaluation of protein thermal stabilities.[16,17]

Below, we describe the development of a highly parallel variable-temperature electrospray ionization mass spectrometry (vT-ESI-MS) approach that is capable of monitoring thermal transitions in mixtures of proteins. We demonstrate the utility of our approach by analyzing mixtures of ribosomal proteins in a single experiment with MS-grade sensitivity and specificity. We anticipate its use for characterizing structural transitions that occur with temperature for large mixtures of proteins in a proteome—that is, the *stabilitome*, and an example of this type of analysis on a fraction of proteins from an *Escherichia coli* lysate is briefly illustrated.

This work builds upon a number of elegant studies involving mass spectrometric analysis of proteins.[18−23] Early proteomics-based workflows leveraged the sensitivity of hydrogen/deuterium exchange patterns to solution temperature to quantify protein thermal stabilities and protein−ligand interactions from biological mixtures.[24] Technical advancements in quantitative proteomics and knowledge of induced stabilization of a protein fold following ligand engagement enabled the unbiased identification of protein−ligand interactions in yeast cell lysates (e.g., stability of proteins from rates of oxidation or SPROX)[25,26] as well as cancer drugs in cultured cells.[27] Enhancements in throughput, sensitivity, and other sample preparation strategies (e.g., advancements in isotope labeling strategies)[28] facilitate deep investigations into thermal stabilities for proteins and protein−ligand interactions present in complex mixtures by following changes in proteolytic

Received: February 19, 2021
Accepted: May 27, 2021
Published: June 8, 2021

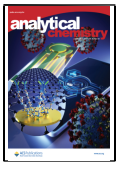

https://doi.org/10.1021/acs.analchem.1c00772
Anal. Chem. 2021, 93, 8484−8492

fragments [e.g., limited-proteolysis (LiP)-MS],[29,30] isotope tag abundances [e.g., thermal proteome profiling (TPP)],[31] and protein solubilities (e.g., SPROX)[32] as the temperature is increased. In many ways, these pioneering studies have matured into robust, discovery-based workflows that can provide a comprehensive survey of hundreds to thousands of protein thermal stabilities in a single experiment. However, at present, these workflows cannot directly account for the impact that protein−protein or protein−small molecule interactions have on stability, as well as protein thermal stabilities modulated by post-translational modifications. Additionally, because proteomics-based techniques require database matching for the identification of experimental findings, it is challenging to identify and validate uncharacterized protein−protein and protein−ligand interactions.

Recently, several groups have developed and applied vT-ESI-MS methods to study the temperature dependence of protein (un)folding,[33−41] protein−ligand interactions in solution,[42,43] as well as kinetic studies that have led to a detailed understanding of the driving forces associated with structural transitions.[44] These studies suggest that it should be possible to analyze mixtures of intact proteins and protein complexes in parallel by following changes in charge state distributions with temperature.[45,46] While the relatively well-defined nature of the ribosomal protein mixture described in this study allows us to characterize different species based on precursor mass characterization, we note that the approach is well suited for top-down MS identification.[47−50] The proof-of-concept study presented below indicates that structural transitions of native protein monomers, as well as protein−ligand and protein−protein complexes, can be determined. Our ability to follow structural transitions prior to protein precipitation (e.g., a phase transition)[31] provides an additional layer of detail to the expansive *meltome atlas* by the capture of thermally induced conformational changes which occur prior to temperature-dependent changes in solubility.

EXPERIMENTAL SECTION

Sample and Reagent Preparation. All solvents were of the highest purity. RNAse-free DNAse was obtained from New England Biolabs. Protein standards (e.g., ubiquitin, lysozyme, and carbonic anhydrase) and RNAse-free sucrose were obtained from Sigma-Aldrich. *E. coli* strain MRE600 was obtained from ATCC (NCTC 8164), and BL21(DE3) was purchased from New England Biolabs.

Cell Growth and Lysis. Cells were streaked onto lysogeny broth (LB) agar plates and incubated overnight at 37 °C. Single colonies were picked and used to inoculate 50 mL of an overnight LB culture. 10 mL of the overnight culture was used to inoculate 1 L of LB broth. Cultures were grown to the mid log phase ($OD_{600} \sim 0.5$) and then harvested by centrifugation (5000 × *g*, 4 °C). Cell pellets were washed twice with distilled water before flash freezing in liquid nitrogen using a previously described procedure.[51] Briefly, a 25 mL syringe was filled with cell paste, which was expelled directly into a 50 mL conical tube filled with liquid nitrogen. The flash-frozen cell "noodles" were crushed with a spatula before being cryogenically ground using a 6875 freezer/mill (SPEX, Metuchen, NJ). The resulting cell powder was stored at −80 °C until use. We also investigated harsher but more complete techniques for mechanical cell lysis to extract proteins and found no noticeable difference except an increased protein yield.

Ribosome Isolation. *E. coli* ribosomes were isolated from strain MRE600 according to the procedure outlined by Rivera and co-workers.[52] Lysed cells were resuspended in a high-Mg^{2+} buffer (20 mM Tris−HCl pH 7.5, 50 mM $MgOAc_2$, 100 mM NH_4Cl, 1 mM DTT, 0.5 mM EDTA, and 1 mM $CaCl_2$). Genomic DNA was digested by the incubation of clarified lysates with 5−10 U/mL of DNAse at 4 °C. The lysates were then subjected to ultracentrifugation at 100,000 × *g* over a high-salt sucrose cushion buffer (37% w/w sucrose, 20 mM Tris−HCl pH 7.5, 50 mM $MgOAc_2$, 100 mM NH_4Cl, 1 mM DTT, and 0.5 mM EDTA) for 17 h. Pelleted ribosomes were resuspended in two volumes of high-Mg^{2+} resuspension buffer. The presence of the 30S, 50S, and 70S complexes was verified by buffer exchanging resuspended ribosomes into the dissociation buffer (20 mM Tris−HCl pH 7.5, 1 mM $MgOAc_2$, 100 mM NH_4Cl, 1 mM DTT, and 0.5 mM EDTA) before analysis.

Preparation of Ribosomal Proteins. The procedure outlined by Talkington et al. was followed to isolate RNA from ribosomal proteins.[53] Briefly, 1 vol of LiCl/urea buffer (8 M urea, 6M LiCl, 25 mM Tris−HCl pH 7.5, 100 mM KCl, and 20 mM $MgCl_2$ 2 mM DTT) was added to a solution of dissociated ribosomes. After overnight incubation at 4 °C, the precipitated 16S rRNA was pelleted at 16,000 × *g* for 10 min. The remaining RNA was precipitated from the supernatant by overnight dialysis in 10 mM ammonium acetate (pH = 7.1) in a 3 kDa dialysis cartridge (Thermo Scientific, Bedford, MA). The precipitated RNA was pelleted by 16,000 × *g* for 10 min. The supernatant was concentrated and desalted using Amicon 3 kDa MWCO filters. Protein concentrations were estimated by nanodrop.

Size Exclusion Chromatography. Cell powders from cryogenic grinding of strain BL21-DE3 were resuspended in five volumes of size exclusion chromatography (SEC) buffer (150 mM NH_4OAc pH = 7.1) supplemented with an EDTA-free protease inhibitor tablet (Roche). Lysates were clarified by centrifugation (20,000 × *g*, 60 min, 4 °C). The clarified lysates were passed through a 0.22 μm filter to further remove particulate and unbroken cells. Protein concentration was determined using a Bradford assay and adjusted to 2−10 mg mL^{-1} using an Amicon 10 kDa MWCO filter. 500 μL aliquots were loaded onto a Superdex 200 15/300 GL size exclusion column equilibrated with SEC buffer connected to an Akta Pure FPLC system (GE Healthcare). Fractions were collected in 0.25 mL aliquots using a 0.4 mL min^{-1} flow rate. Fractions from 5 to 10 SEC runs were pooled and concentrated to 1−3 mg mL^{-1} before MS analysis.

Mass Spectrometry. MS studies were carried out using a Synapt G2 MS system tuned to minimize unwanted high-energy collisions. Briefly, the skimmer cone voltage: 20−60 V, extraction cone voltage: 1−2 V, source temperature: 30−50 °C, trap DC bias: 30−35 V, trap pressure: 0.042 mbar, and backing pressure: 5−10 mbar. The instrument was operated in the resolution mode; polarities were set to transmit and detect positive ions. The manufacturer electrospray ionization source was removed and interlocks overridden to allow for coupling of a prototype vT-ESI source, described in more detail previously.[54] 10−30 μL of the analyte solution was inserted into borosilicate capillaries pulled to 1−5 μm using a P97 Flaming/Brown micropipette puller (Sutter Instruments, Novato, CA). A 0.6−1.1 kV electric potential was applied to the platinum electrode in contact with the solution to initiate the formation of an electrospray. Mass spectra were collected

https://doi.org/10.1021/acs.analchem.1c00772
Anal. Chem. 2021, 93, 8484−8492

in 1 or 2 °C increments starting from room temperature until a stable electrospray could no longer be maintained. Each spectrum was collected for 1.0 min and represents the average of 60 scans.

Charge Detection Mass Spectrometry. Charge detection mass spectrometry (CDMS) was carried out on a home-built instrument described in detail elsewhere.[55] Samples were electrosprayed into a heated capillary using a Triversa Nanomate (Advion, Ithaca, NY). After passing through three differentially pumped regions, ions are accelerated by a 100 V potential before being energy-selected (~100 eV/charge) by a dual-hemispherical deflection analyzer. Single ions within this narrow band of kinetic energy were subsequently trapped in a linear ion trap containing the charge conducting cylinder. The trapping period was set to 100 ms. The periodic signal was analyzed using fast Fourier transform by a Fortran program written in-house.[56] Subsequent data processing was carried out using OriginPro (OriginLab, Northampton, MA).

Bottom-Up Liquid Chromatography–MS Proteomics. Aliquots of protein solutions (~10–50 μg) were dried using a vacuum concentrator. Proteins were dissolved in 8 M urea (in 100 mM ammonium bicarbonate, pH 7.5, Sigma-Aldrich, St. Louis, MO, U.S.A) and placed in an ultrasonic bath for 10 min. Disulfide bonds were reduced using tris 2-carboxyethyl phosphine hydrochloride (2 mM, Sigma-Aldrich, St. Louis, MO, U.S.A) at 56 °C for 1 h. Reduced cysteines were then alkylated using iodoacetamide (4 mM, Sigma-Aldrich, St. Louis, MO, U.S.A) at room temperature for 1 h in the dark. The solution was diluted to 1 M urea with 100 mM ammonium bicarbonate (pH 7.5, Sigma-Aldrich, St. Louis, MO, U.S.A.) before the addition of trypsin (1:100 w/w, modified sequencing grade trypsin, Promega, Madison, WI, U.S.A) for overnight digestion at 37 °C. Peptides were desalted using C-18 Zip Tip (MilliporeSigma, Burlington, MA, U.S.A.) and dried on a vacuum concentrator. Desalted peptides were resolubilized in buffer A (0.1% formic acid, H_2O, Fisher Scientific, Hanover, NH) and loaded onto a reverse-phase trap column (Acclaim PepMap 100, 75 μm × 2 cm, nanoviper, C18, 3 μm, 100 Å, ThermoFisher, Waltham, MA, U.S.A) using an EasyNanoLC 1200 (ThermoFisher, Waltham, MA, U.S.A.) for 10 μL at a flow rate of 5 μL/min. Trapped peptides were then analytically separated (Acclaim PepMap RSLC, 75 μm × 25 cm, 2 μm, 100 Å, ThermoFisher, Waltham, MA, U.S.A) using a 120 min linear gradient of 7–38% buffer B (0.1% formic acid, 80% acetonitrile, 20% H_2O, Fisher Scientific, Hanover, NH) at a flow rate of 300 nL/min. Separated peptides were then electrosprayed in the positive mode into a Fusion Lumos Tribrid (ThermoFisher, Waltham, MA, U.S.A.) mass spectrometer operated in the data-dependent mode (3 s cycle time). Precursor mass analysis occurred in the Orbitrap analyzer (Orbitrap resolution: 120,000 @ 200 m/z, scan range: 400–2000 m/z), while subsequent tandem mass scans occurred in the ion trap. Fragment ion spectra were generated using higher energy dissociation (HCD collision energy = 32%) on high intensity (intensity threshold: 2.5×10^4) and multiply charged ions (charge state = 2–7). Quadrupole isolation of precursors was completed with a 0.5 mass-to-charge (m/z) offset and an isolation window of 0.7 m/z. Additional MS/MS scans of precursor ions within 10 ppm were dynamically excluded after the initial scan for 30 s. Tandem mass scans were acquired with an AGC setting of 5×10^4 or a maximum fill time of 150 ms. Liquid chromatography–MS (LC–MS) data were searched against the SEQUEST database using Proteome Discoverer.

Data Analysis. To provide a list of possible protein identifications, the mass spectra collected at room temperature were deconvoluted using UniDec[57] and compared to the top 20 most abundant proteins identified by bottom-up sequencing (estimated abundances for each protein group). The spectra were then manually searched for predicted m/z values pertaining to each possible protein. All processed (e.g., cleavage of initiator Met, Lys methylation), oligomeric, and ligand-bound forms of the proteins identified by LC–MS were considered and manually validated based on Uniprot entries. Once a series of three or more adjacent charge states were identified, integrated areas for the peaks for the charge states present at room temperature were summed at each temperature and used to infer the loss of the native state. In some cases, the high charge state products of melting could be easily identified, in which case the melting curves are determined by the calculation of the weighted average charge state at each temperature. The data points were fit to a sigmoidal function[33,54] to determine the T_m. The oligomeric states for any multimeric forms were verified by MS/MS *via* collision-induced dissociation (CID) of selected precursor ions. Experiments were collected in duplicate (two biological replicates), and uncertainties are reported as standard deviations from $n = 2$ measurements. All data sets were processed and plotted using OriginPro (OriginLab, Northampton, MA).

RESULTS AND DISCUSSION

Analysis of Ribosomal Protein Heterogeneity. A series of confirmatory experiments were carried out to confirm the presence and validate the purity of the ribosomal proteins. Figure 1a shows a CDMS spectrum for ribosomes in a buffer containing a low concentration of Mg^{2+} salt, which promotes the dissociation of the 70S complex into the 30S and 50S subunits. The three peaks, centered at 0.97, 1.56, and 2.47 MDa, correspond to the 30S, 50S, and 70S ribosomal species, respectively. Overlaid in red, blue, and green are the predicted peak shapes for homogeneous distributions of the 30S, 50S, and 70S particles, respectively. The measured peak centers are ~10% heavier than the anticipated molecular weights.[58] A small amount of this excess mass may be due to residual salt and counterions that persist following the intact ionization of the ribosomal subunits; however, this is expected to contribute ~2–3 kDa (~0.1%).[59,60] The remaining excess mass indicates that accessory proteins and ribonucleic acids have co-purified with the 70S species. The peak broadening observed in the experimental spectrum is clearly reflective of this heterogeneity. Nonetheless, the presence of these three signals provides evidence for purified intact ribosomal particles.

Following centrifugal enrichment, this sample was analyzed using a LC–MS-based shotgun proteomics approach to identify the proteins present. As shown in Figure 1b, ~600 proteins were identified—all ribosomal proteins were detected, confirming the successful fractionation of the ribosome. The proteins enriched after rRNA removal were identified by sorting the list of proteins by their LC–MS abundances (Figure 1b and Table S2), confirming the successful fractionation of ribosomal particles from the cellular milieu. Protein subunits were released from the 30S and 50S ribosomal subcomplexes by rRNA precipitation, and the resulting sample was subjected to mass spectrometric analysis.

https://doi.org/10.1021/acs.analchem.1c00772
Anal. Chem. 2021, 93, 8484–8492

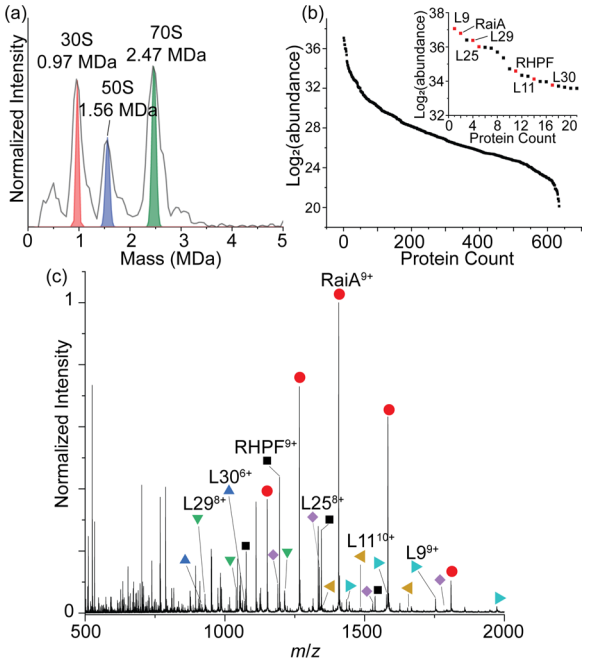

Figure 1. Analysis of enriched ribosomal proteins. (a) CDMS spectrum for intact ribosomal particles in a low-concentration Mg^{2+} buffer. The signals at 0.97, 1.56, and 2.47 MDa correspond to the 30S, 50S, and 70S ribosomal particles, respectively. (b) LC−MS shotgun proteomic analysis of the enriched ribosomal particles ranked by the estimated protein abundance. The inset shows the top 20 most abundant proteins. (c) Mass spectrum for ribosomal proteins collected after rRNA precipitation. Seven species, L9, L25, RaiA, L25, RHPF, L11, and L30, were readily identified.

Figure 1c shows a mass spectrum collected at room temperature (~26 °C). Hundreds of signals are present, most of which have well-resolved isotopic envelopes. A combination of spectral deconvolution and manual peak assignment was used to identify signals that arise from a single species. Using this approach, we readily identified several peak series that correspond to 7 of the 20 most abundant proteins, all of which are labeled in Figure 1c and listed in Table S1. We anticipate that the unassigned signals in our mass spectrum pertain to protein−protein and protein−ligand complexes, as well as species with different protein post-translational modifications that would result in a deviation from the anticipated sequence mass; advances in "native top-down" approaches would further our ability to characterize the signals pertaining to proteins with such slight compositional differences.[61,62]

Thermal Denaturation of *E. coli* Ribosomal Proteins. Following our three-tiered approach for protein identification, we used a prototype vT-ESI source[54] to incrementally heat the protein solution prior to MS analysis. Figure 2a shows representative mass spectra collected at solution temperatures of 26 and 88 °C. At low solution temperatures, predominantly low-charge species are present; isotopic envelopes pertaining to z = 5 to z = 12 are observed. This is expected for folded proteins with molecular weights <20 kDa. For the seven proteins we identified, we did not observe evidence for dominant high charge state signals (z > 13) in the low-temperature mass spectrum, indicating that these species are in compact, folded configurations with basic, surface-exposed residues protonated.

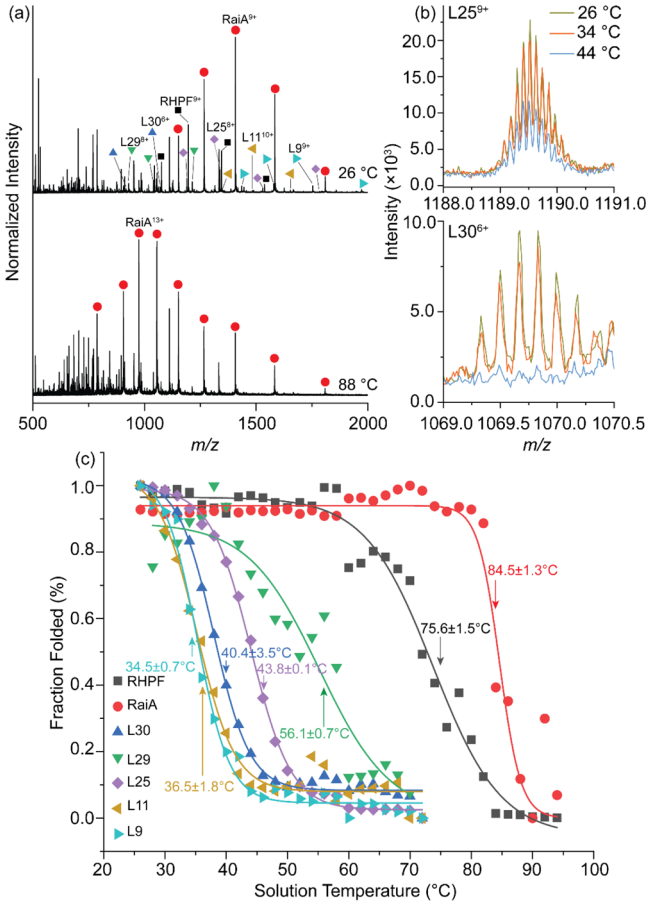

Figure 2. vT-ESI-MS analysis of endogenous ribosomal proteins. (a) Mass spectra at 26 and 88 °C. A shift from low to high charge state for RaiA is clearly identified. (b) Mass spectra for the 9+ charge state of L25 and 6+ charge state of L30 at three representative solution temperatures. Increases in solution temperature show a concomitant decrease in the absolute ion intensity. (c) Melting curves for each of the seven species we identified. The curve for RaiA was determined by the calculation of the weighted average charge state, which reports on the fraction of unfolded protein. We determined the fraction folded for the other species by summing the ion intensities for the respective low charge state ions identified at 26 °C for each protein and then normalized these values between 0 and 1 using the least and most intense data points across the melting transition. For these cases, the intensities of ≥3 adjacent charge states present at low solution temperatures were summed at each temperature point. Values are reported as the average and standard deviation from n = 2 biological replicates.

As the solution temperature is increased, there is a decrease in ion intensity for the low charge state signals. For the highly abundant protein ribosome-associated initiation factor A (RaiA), a shift from low to high m/z ratios is observed. As shown in Figure 2a, the charge state envelope for RaiA shifts from favoring $[M + 9H]^{9+}$ at T = 26 °C to $[M + 13H]^{13+}$ at T = 88 °C. This shift in protein charge state signifies an unfolding transition—as the protein denatures with increases in solution temperature, basic core residues become solvent-exposed and acquire a charge.[33,63] Analyses of these data involve plotting the weighted average charge state as a function of solution temperature to track the protein unfolding transition. The high charge state peak series for the other six proteins that we identified overlap significantly, making it challenging to distinguish between signals from multiple protein ions.

https://doi.org/10.1021/acs.analchem.1c00772
Anal. Chem. 2021, 93, 8484−8492

Therefore, to quantify the amount of each folded protein at each temperature for the remaining six proteins, we followed the change in absolute ion abundance for the assigned low charge state signals at each solution temperature. This strategy is similar to approaches used to quantify changes in peptide[29] and reporter ion intensities,[27] as well as contemporary techniques such as microscale thermophoresis and differential scanning fluorimetry. Identification of the folded and unfolded populations is a major technical advantage over traditional biophysical approaches to study folding, as we and others have outlined in previous work.[33−43] As a control vT-ESI-MS experiment, we tested whether these approaches provide different T_m values for individual proteins in dilute solutions and find very close agreement in the measured values (Figure S1). In addition, good agreement between measured T_m values and those reported in the literature is obtained upon characterization of a simple mixture of standard proteins (Figure S2). While it is preferable to utilize average charge state shifts to follow unfolding, it is challenging to capture this level of detail for mixtures of denatured proteins where high charge state signals overlap (Figure 2a, 88 °C); we present here an alternative means which readily allows for the identification of T_m values from mixtures of proteins. Figure 2b shows two representative examples illustrating this approach—the intensity for the 9+ charge state of the large ribosomal protein subunit L25 gradually decreases as the solution temperature is increased. A similar phenomenon is observed for the 6+ charge state of the large ribosomal protein subunit L30, albeit with a different temperature dependence on the signal intensity. The increase in charge state or decrease in the intensity of the low charge state species is a clear indication that the protein has undergone a melting transition in solution.

Figure 2c shows a plot depicting the fraction folded for each protein at each solution temperature (i.e., melting curves). As anticipated, the fraction of folded protein tends to low values as the temperature is increased. The T_m for each system, which provides an overall signature of stability for the folded protein, is derived by obtaining the midpoint of a sigmoidal fit to the data, as shown in the figure. RaiA appears to be the most stable with a T_m = 84.5 ± 1.3 °C, while the large ribosomal protein subunit L9 is the least stable with T_m = 34.5 ± 0.7 °C. It is remarkable that the melting curves in Figure 2c are distinct as this is a clear indication that melting transitions can be captured for individual species present within complex mixtures. These well-defined melting temperatures and associated uncertainties are summarized in Table S1.

Our approach of measuring protein behavior in a complex mixture allows for insights into environmental changes and interactions within the proteome that may affect protein stability. Large ribosomal protein subunits L9, L11, L30, and L25 have melting temperatures near or slightly above 37 °C. This is remarkably close to the optimal growth temperature for *E. coli*. In the absence of stabilizing rRNA (and other noncovalent interactions), this suggests that life beyond the optimal growth temperature is unsustainable due to the inhibition of the protein synthesis machinery.[64] This is consistent with calculations by Ghosh et al., who suggested that global protein stabilities predicted based on sequences alone are quite low.[1] They suggest that at temperatures above 43 °C, it is protein unfolding transitions rather than membrane restructuring that drives the cell to create an intracellular environment that cannot support life. These stabilities may be affected by interactions with other host cell factors. For example, L9 is known to directly interact with the 3′-end of the 23S rRNA. The lower T_m for this species signifies that these protein−RNA interactions are critical for stabilizing the fold of L9,[65] suggesting that the *in vivo* folded−unfolded equilibria are delicately balanced and can be modulated along the many layers within cellular interaction networks.

Proof-of-Concept Extension Involving a Hybrid MS-Based Analysis of an *E. coli* Lysate Fraction. Now that we have demonstrated the ability to monitor structural transitions in mixtures based on the relatively well-defined set of ribosomal proteins, it is interesting to extend this to a proteome generated upon the cell lysis of *E. coli*. Figure 3a shows the SEC trace collected for the separation of soluble proteins harvested from cell lysates. Three features are observed between the void (~8.5 mL) and retained (~22 mL) volumes. Estimation of the molecular weights using a set of proteins with known molecular weights indicates that the middle feature corresponds to proteins weighing ~75 kDa. Figure 3b shows a plot of the estimated protein abundances for the ~1000 different proteins we identified in the ~75 kDa fraction by LC−MS-based shotgun proteomics (see Table S3). Interestingly, the molecular weights for each protein we sequenced are centered between 35 and 40 kDa, indicating that the proteins we have captured in this SEC fraction are predominantly dimeric.

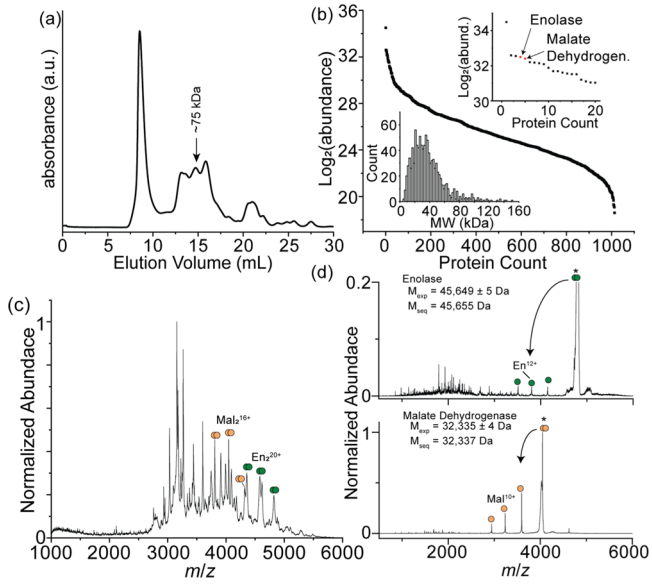

Figure 3. Analysis of fractionated *E. coli* lysate. (a) Representative SEC trace for whole-cell lysate. The feature corresponding to an estimated molecular weight of 75 kDa was analyzed. (b) LC−MS shotgun proteomic analysis of the 75 kDa SEC fraction, ranked by estimated protein abundance. The inset shows a detailed view of the top 20 proteins. The inset (bottom) shows a histogram of the molecular weights for each protein group, which are centered near ~30 kDa. (c) Mass spectrum for the 75 kDa fraction. Peaks assigned by (d) tandem MS by CID.

Figure 3c shows a mass spectrum collected at 30 °C. This mass spectrum is much more complicated than that for the isolated ribosomal proteins; none of the ~100 peaks have resolved isotopic envelopes, and many features are broad resulting from overlapping signals. This makes intact mass determination nontrivial. Spectral deconvolution[57] was inconclusive, likely due to the complexity of these data sets and the

https://doi.org/10.1021/acs.analchem.1c00772
Anal. Chem. 2021, 93, 8484−8492

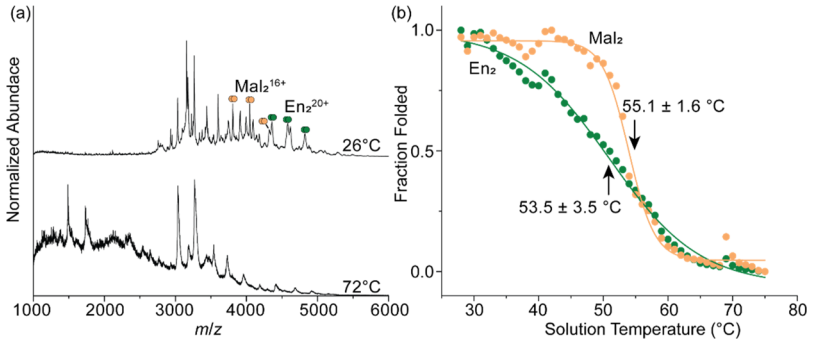

Figure 4. Thermal denaturation of the fractionated lysate. (a) Representative mass spectra collected at 26 and 72 °C. (b) Melting curves for the two protein complexes Mal_2 and En_2. Melting curves normalized to the most intense data point across the melting transition. We determined the fraction folded by summing the ion intensities for the respective low charge state ions identified at 26 °C for each protein and then normalized these values between 0 and 1 using the least and most intense data points across the melting transition. For these cases, the intensities of ≥3 adjacent charge states present at low solution temperatures were summed at each temperature point. Values reported as the average and standard deviation (n = 2 biological replicates).

presence of overlapping features. However, there are several resolved signals that resemble a charge state series—namely, peaks between ∼3500 and 5000 m/z. Each discernible peak was selected using the quadrupole and fragmented using CID to interrogate the chemical identity of the features in this region. The MS/MS spectra shown in Figure 3d are signatures of the protein complex fragmentation—that is, monomer ejection amid additional fragment ions.[66,67] Corroboration of the masses of these monomers with the highly abundant proteins identified by LC−MS provides a straightforward means to determine the chemical identity of several of these signals. Specifically, two species that we identified using this tandem MS approach were dimeric malate dehydrogenase (Mal_2) and enolase (En_2). Both protein complexes carry out important catalytic roles in glycolysis and are known to form functional dimers. We therefore sought to characterize the thermal stabilities of these two proteins using our vT-ESI-MS approach.

Thermal Denaturation of *E. coli* Cell Lysate. Figure 4a shows mass spectra collected at 30 and 72 °C. As the solution temperature is increased, there is a decrease in the signals at high m/z (including those for Mal_2 and En_2) and a concomitant increase in intensity of the low m/z species. This is a clear indication that melting transitions have occurred. Similar to the mixture of ribosomal proteins, the spectral congestion at low m/z at elevated temperatures makes it challenging to confidently assign the high charge state products of melting. However, there is a systematic decrease in the precursor peak intensity as the solution temperature is increased. Figure 4b shows plots of the decay in the precursor ion intensity for Mal_2 and En_2, which report on the fraction of the assembled protein complexes. The sigmoidal shape of these plots is a signature for cooperative melting transitions, and the steepness is indicative of differences in the degree of cooperativity. Signals for the enolase dimer undergo a gradual decrease in intensity between $T \sim 30$ and 70 °C, with T_m = 53.5 ± 3.5 °C. In contrast, the curve for dimeric malate dehydrogenase is sharp—decreasing in intensity between $T \sim$ 50 and 60 °C with T_m = 55.1 ± 1.6 °C. We surmise that Mal_2 disassembles *via* a highly cooperative transition coupled to the unfolding of monomeric subunits, while En_2 undergoes controlled dissociation to intact monomers. This is consistent with the collisional activation studies presented in Figure 3d. Mal_2 ions almost completely dissociate into highly charged monomers by 80 V; however, even at the highest instrumentally accessible collision voltage (200 V), En_2^{19+} precursor ions remain the most abundant species in the mass spectrum.

CONCLUSIONS

vT-ESI-MS was demonstrated as a means of characterizing melting transitions for isolated ribosomal proteins. The method was extended to an *E. coli* lysate where two protein complexes were identified and characterized. In this approach, as the solution temperature is increased, proteins and protein complexes undergo structural and organizational transitions that are monitored based on changes in charge state distributions. Compared with classical methods, the vT-ESI-MS approach is substantially more sensitive and is capable of monitoring multiple structural transitions for different species simultaneously. This is an important step for advancing these techniques as a means of characterizing large numbers of stabilities associated with proteins in a proteome, and as with the development of the pan-species *meltome via* TPP,[31] we anticipate the emerging area of *stabilitomics*, which will fill an important gap in understanding the crosstalk between protein complex stability, structural changes, and post-translational modifications.

Although this method illustrates key first steps toward the proteome-wide characterization of protein stabilities, the issue of characterizing structural properties of proteins in complex mixtures *via* MS remains challenging. Overlapping signals within the MS spectra require manual inspection of the data to accurately assign protein identification. Instrumental tuning, in particular gentle source conditions, is imperative to maintain conformations and stabilities of proteins that resemble those in solution. Further studies are needed to explore additional limitations of this hybrid MS workflow, but the present study offers a promising outlook. Namely, our studies show that the structures of lysate proteins En_2 and Mal_2 are affected in a similar manner by changes in solution temperature as well as gas-phase energization, leading to the exciting possibility that this approach may also be suitable to assess links between gas-phase and solution-phase energy landscapes. Generation of libraries of T_m values and collision-induced unfolding midpoints[23,68] for multiple proteins in a single experiment will provide a fruitful avenue to further these endeavors.

https://doi.org/10.1021/acs.analchem.1c00772
Anal. Chem. 2021, 93, 8484−8492

Incorporation of high-resolution ion mobility spectrometry,[35] structural proteomics,[29] and novel MS/MS methodologies (e.g., proton transfer charge reduction/CID,[69] SWATH[70]) provide new means to characterize structural and compositional changes involved with thermal denaturation for many species in a parallel fashion. In many ways, the adaptation of sample preparation workflows developed for proteomics-based approaches[24−32] with our vT-ESI-MS technique described herein places MS-based stability measurements at an optimal vantage point to delineate composition and structural changes for proteins from nearly natural environments. This includes the characterization of biomolecular interactions that are proteoform-specific.[71] Inclusion of these complimentary tools, that each identify different aspects of biomolecular structure and function, provides a new perspective toward the stability networks present within proteomes—*stabilitomes*.

■ ASSOCIATED CONTENT

Supporting Information

The Supporting Information is available free of charge at https://pubs.acs.org/doi/10.1021/acs.analchem.1c00772.

Control experiment detailing the use of average charge and signal decay as a proxy for unfolding; control experiment detailing the ability to characterize T_m values for a simple mixture of standard proteins; and report of ribosomal and cell lysate proteins identified and their T_m values (PDF)

Report of ribosomal proteins identified by LC−MS (XLSX)

Report of proteins identified by LC−MS in size-fractionated lysate (XLSX)

■ AUTHOR INFORMATION

Corresponding Author

David E. Clemmer − *Department of Chemistry, Indiana University, Bloomington, Indiana 47401, United States;* orcid.org/0000-0003-4039-1360; Email: clemmer@indiana.edu

Authors

Tarick J. El-Baba − *Department of Chemistry, Indiana University, Bloomington, Indiana 47401, United States;* Present Address: Physical and Theoretical Chemistry Laboratory, University of Oxford, S Parks Rd, Oxford OX1 3QZ.

Shannon A. Raab − *Department of Chemistry, Indiana University, Bloomington, Indiana 47401, United States*

Rachel P. Buckley − *Department of Chemistry, Indiana University, Bloomington, Indiana 47401, United States*

Christopher J. Brown − *Department of Chemistry, Indiana University, Bloomington, Indiana 47401, United States;* Present Address: Corteva Agriscience, Zionsville Rd, Indianapolis, Indiana 46268, United States.

Corinne A. Lutomski − *Department of Chemistry, Indiana University, Bloomington, Indiana 47401, United States;* Present Address: Physical and Theoretical Chemistry Laboratory, University of Oxford, S Parks Rd, Oxford OX1 3QZ.

Lucas W. Henderson − *Department of Chemistry, Indiana University, Bloomington, Indiana 47401, United States*

Daniel W. Woodall − *Department of Chemistry, Indiana University, Bloomington, Indiana 47401, United States;* Present Address: Amgen, Inc., Amgen Center Dr, Thousand Oaks, California 91320, United States.

Jiangchuan Shen − *Department of Molecular and Cellular Biochemistry, Indiana University, Bloomington, Indiana 47401, United States*

Jonathan C. Trinidad − *Department of Chemistry, Indiana University, Bloomington, Indiana 47401, United States;* orcid.org/0000-0002-8279-1509

Hengyao Niu − *Department of Molecular and Cellular Biochemistry, Indiana University, Bloomington, Indiana 47401, United States*

Martin F. Jarrold − *Department of Chemistry, Indiana University, Bloomington, Indiana 47401, United States;* orcid.org/0000-0001-7084-176X

David H. Russell − *Department of Chemistry, Texas A&M University, College Station, Texas 77843, United States*

Arthur Laganowsky − *Department of Chemistry, Texas A&M University, College Station, Texas 77843, United States;* orcid.org/0000-0001-5012-5547

Complete contact information is available at: https://pubs.acs.org/10.1021/acs.analchem.1c00772

Author Contributions

‖These authors contributed equally to this study.

Notes

The authors declare no competing financial interest.

■ ACKNOWLEDGMENTS

This work was supported by funds from the NIH (5R01GM117207-04, 5R01GM121751-02, and 1R01GM131100-01). The authors would like to thank Dr. Giovanni Gonzalez-Gutierrez, Kathleen Grassmyer, and Yixiang Zhang for their technical expertise.

■ REFERENCES

(1) Ghosh, K.; de Graff, A. M. R.; Sawle, L.; Dill, K. A. *J. Phys. Chem. B* **2016**, *120*, 9549−9563.

(2) Santra, M.; Dill, K. A.; de Graff, A. M. R. *Proc. Natl. Acad. Sci. U.S.A.* **2019**, *116*, 22173−22178.

(3) Hipp, M. S.; Kasturi, P.; Hartl, F. U. *Nat. Rev. Mol. Cell Biol.* **2019**, *20*, 421−435.

(4) Price, J. C.; Guan, S.; Burlingame, A.; Prusiner, S. B.; Ghaemmaghami, S. *Proc. Natl. Acad. Sci. U.S.A.* **2010**, *107*, 14508−14513.

(5) Fornasiero, E. F.; Mandad, S.; Wildhagen, H.; Alevra, M.; Rammner, B.; Keihani, S.; Opazo, F.; Urban, I.; Ischebeck, T.; Sakib, M. S.; Fard, M. K.; Kirli, K.; Centeno, T. P.; Vidal, R. O.; Rahman, R. U.; Benito, E.; Fischer, A.; Dennerlein, S.; Rehling, P.; Feussner, I.; Bonn, S.; Simons, M.; Urlaub, H.; Rizzoli, S. O. *Nat. Commun.* **2018**, *9*, 4230.

(6) Leavitt, S.; Freire, E. *Curr. Opin. Struct. Biol.* **2001**, *11*, 560−566.

(7) Greenfield, N. J. *Nat. Protoc.* **2006**, *1*, 2527−2535.

(8) Wand, A. J. *Nat. Struct. Biol.* **2001**, *8*, 926−931.

(9) Puglisi, R.; Brylski, O.; Alfano, C.; Martin, S. R.; Pastore, A.; Temussi, P. A. *Commun. Chem.* **2020**, *3*, 100.

(10) Boulet-Audet, M.; Byrne, B.; Kazarian, S. G. *Anal. Chem.* **2014**, *86*, 9786−9793.

(11) Jiang, B.; Jain, A.; Lu, Y.; Hoag, S. W. *Pharmaceutics* **2019**, *16*, 3687−3693.

(12) Liu, W.-W.; Zhu, Y.; Fang, Q. *Anal. Chem.* **2017**, *89*, 6678−6685.

(13) Johnson, C. M. *Arch. Biochem. Biophys.* **2013**, *531*, 100−109.

(14) Matulis, D.; Kranz, J. K.; Salemme, F. R.; Todd, M. J. *Biochem* **2005**, *44*, 5258−5266.
(15) Wintrode, P. L.; Makhatadze, G. I.; Privalov, P. L. *Proteins* **1994**, *18*, 246−253.
(16) Ibarra-Molero, B.; Naganathan, A. N.; Sanchez-Ruiz, J. M.; Muñoz, V. *Methods Enzymol.* **2016**, *567*, 281−318.
(17) Torres, F. E.; Recht, M. I.; Coyle, J. E.; Bruce, R. H.; Williams, G. *Curr. Opin. Struct. Biol.* **2010**, *20*, 598−605.
(18) Bohrer, B. C.; Merenbloom, S. I.; Koeniger, S. L.; Hilderbrand, A. E.; Clemmer, D. E. *Annu. Rev. Anal. Chem.* **2008**, *1*, 293−327.
(19) Chorev, D. S.; Baker, L. A.; Wu, D.; Beilsten-Edmands, V.; Rouse, S. L.; Zeev-Ben-Mordehai, T.; Jiko, C.; Samsudin, F.; Gerle, C.; Khalid, S.; Stewart, A. G.; Matthews, S. J.; Grünewald, K.; Robinson, C. V. *Science* **2018**, *362*, 829−834.
(20) Wyttenbach, T.; Bowers, M. T. *J. Phys. Chem. B* **2011**, *115*, 12266−12275.
(21) Anderson, L.; Hunter, C. L. *Mol. Cell. Proteomics* **2006**, *5*, 573−588.
(22) Heck, A. J. R. *Nat. Methods* **2008**, *5*, 927−933.
(23) Dixit, S. M.; Polasky, D. A.; Ruotolo, B. T. *Curr. Opin. Chem. Biol.* **2018**, *42*, 93−100.
(24) Ghaemmaghami, S.; Fitzgerald, M. C.; Oas, T. G. *Proc. Natl. Acad. Sci. U.S.A.* **2000**, *97*, 8296−8301.
(25) West, G. M.; Tucker, C. L.; Xu, T.; Park, S. K.; Han, X.; Yates, J. R., III; Fitzgerald, M. C. *Proc. Natl. Acad. Sci. U.S.A.* **2010**, *107*, 9078−9082.
(26) Strickland, E. C.; Geer, M. A.; Tran, D. T.; Adhikari, J.; West, G. M.; DeArmond, P. D.; Xu, Y.; Fitzgerald, M. C. *Nat. Protoc.* **2013**, *8*, 148−161.
(27) Savitski, M. M.; Reinhard, F. B. M.; Franken, H.; Werner, T.; Savitski, M. F.; Eberhard, D.; Molina, D. M.; Jafari, R.; Dovega, R. B.; Klaeger, S.; Kuster, B.; Nordlund, P.; Bantscheff, M.; Drewes, G. *Science* **2014**, *346*, 1255784.
(28) Ting, L.; Rad, R.; Gygi, S. P.; Haas, W. *Nat. Methods* **2011**, *8*, 937−940.
(29) Leuenberger, P.; Ganscha, S.; Kahraman, A.; Cappelletti, V.; Boersema, P. J.; von Mering, C.; Claassen, M.; Picotti, P. *Science* **2017**, *355*, No. eaai7825.
(30) Volkening, J. D.; Stecker, K. E.; Sussman, M. R. *Mol. Cell. Proteomics* **2019**, *18*, 308−319.
(31) Jarzab, A.; et al. *Nat. Methods* **2020**, *17*, 495−503.
(32) Meng, H.; Ma, R.; Fitzgerald, M. C. *Anal. Chem.* **2018**, *90*, 9249−9255.
(33) El-Baba, T. J.; Woodall, D. W.; Raab, S. A.; Fuller, D. R.; Laganowsky, A.; Russell, D. H.; Clemmer, D. E. *J. Am. Chem. Soc.* **2017**, *139*, 6306−6309.
(34) Woodall, D. W.; Brown, C. J.; Raab, S. A.; El-Baba, T. J.; Laganowsky, A.; Russell, D. H.; Clemmer, D. E. *Anal. Chem.* **2020**, *92*, 3440−3446.
(35) Raab, S. A.; El-Baba, T. J.; Woodall, D. W.; Liu, W.; Liu, Y.; Baird, Z.; Hales, D. A.; Laganowsky, A.; Russell, D. H.; Clemmer, D. E. *J. Am. Chem. Soc.* **2020**, *142*, 17372−17383.
(36) Fouque, K. D. J.; Fernandez-Lima, F. *J. Phys. Chem. B* **2020**, *124*, 6257−6265.
(37) El-Baba, T. J.; Fuller, D. R.; Woodall, D. W.; Raab, S. A.; Conant, C. R.; Dilger, J. M.; Toker, Y.; Williams, E. R.; Russell, D. H.; Clemmer, D. E. *Chem. Commun.* **2018**, *54*, 3270−3273.
(38) Mirza, U. A.; Cohen, S. L.; Chait, B. T. *Anal. Chem.* **1993**, *65*, 1−6.
(39) Wang, G.; Abzalimov, R. R.; Kaltashov, I. A. *Anal. Chem.* **2011**, *83*, 2870−2876.
(40) Zhao, F.; Matt, S. M.; Bu, J.; Rehrauer, O. G.; Ben-Amotz, D.; McLuckey, S. A. *J. Am. Soc. Mass Spectrom.* **2017**, *28*, 2001−2010.
(41) Mortensen, D. N.; Williams, E. R. *Anal. Chem.* **2015**, *87*, 1281−1287.
(42) Woodall, D. W.; El-Baba, T. J.; Fuller, D. R.; Liu, W.; Brown, C. J.; Laganowsky, A.; Russell, D. H.; Clemmer, D. E. *Anal. Chem.* **2019**, *91*, 6808−6814.
(43) Cong, X.; Liu, Y.; Liu, W.; Liang, X.; Russell, D. H.; Laganowsky, A. *J. Am. Chem. Soc.* **2016**, *138*, 4346−4349.
(44) Marchand, A.; Czar, M. F.; Eggel, E. N.; Kaeslin, J.; Zenobi, R. *Nat. Commun.* **2020**, *11*, 566.
(45) Reid, G. E.; Shang, H.; Hogan, J. M.; Lee, G. U.; McLuckey, S. A. *Anal. Chem.* **2002**, *124*, 7353−7362.
(46) Gan, J.; Ben-Nissan, G.; Arkind, G.; Tarnavsky, M.; Trudeau, D.; Noda Garcia, L.; Tawfik, D. S.; Sharon, M. *Anal. Chem.* **2017**, *89*, 4398−4404.
(47) Breuker, K.; Jin, M.; Han, X.; Jiang, H.; McLafferty, F. W. *J. Am. Soc. Mass Spectrom.* **2008**, *19*, 1045−1053.
(48) Kelleher, N. L. *Anal. Chem.* **2004**, *76*, 196A−203A.
(49) LeDuc, R. D.; Taylor, G. K.; Kim, Y.-B.; Januszyk, T. E.; Bynum, L. H.; Sola, J. V.; Garavelli, J. S.; Kelleher, N. L. *Nucleic Acids Res.* **2004**, *32*, W340−W345.
(50) Wynne, C.; Fenselau, C.; Demirev, P. A.; Edwards, N. *Anal. Chem.* **2009**, *81*, 9633−9642.
(51) See: "Cryogenic Disruption of Yeast Cells" at http://lab.rockefeller.edu/rout/protocols. Protocol was used in: Kim, S. J.; Fernandez-Martinez, J.; Nudelman, I.; Shi, Y.; Zhang, W.; Raveh, B.; Herricks, T.; Slaughter, B. D.; Hogan, J. A.; Upla, P.; Chemmama, I. E.; Pellarin, R.; Echeverria, I.; Shivaraju, M.; Chaudhury, A. S.; Wang, J.; Williams, R.; Unruh, J. R.; Greenberg, C. H.; Jacobs, E. Y.; Yu, Z.; de la Cruz, M. J.; Mironska, R.; Stokes, D. L.; Aitchison, J. D.; Jarrold, M. F.; Gerton, J. L.; Ludtke, S. J.; Akey, C. W.; Chait, B. T.; Sali, A.; Rout, M. P. *Nature* **2018**, *555*, 475−482.
(52) Rivera, M. C.; Maguire, B.; Lake, J. A. *Cold Spring Harb. Protoc.* **2015**, *3*, 293.
(53) Talkington, M. W. T.; Siuzdak, G.; Williamson, J. R. *Nature* **2005**, *438*, 628−632.
(54) El-Baba, T. J.; Clemmer, D. E. *Int. J. Mass Spectrom.* **2019**, *443*, 93−100.
(55) Keifer, D. Z.; Shinholt, D. L.; Jarrold, M. F. *Anal. Chem.* **2015**, *87*, 10330−10337.
(56) Draper, B. E.; Jarrold, M. F. *J. Am. Soc. Mass Spectrom.* **2019**, *30*, 898−904.
(57) Marty, M. T.; Baldwin, A. J.; Marklund, E. G.; Hochberg, G. K. A.; Benesch, J. L. P.; Robinson, C. V. *Anal. Chem.* **2015**, *87*, 4370−4376.
(58) Van de Waterbeemd, M.; Fort, K. L.; Boll, D.; Reinhardt-Szyba, M.; Routh, A.; Makarov, A.; Heck, A. J. R. *Nat. Methods* **2017**, *14*, 283−286.
(59) Keifer, D. Z.; Pierson, E. E.; Hogan, J. A.; Bedwell, G. J.; Prevelige, P. E.; Jarrold, M. F. *Rapid Commun. Mass Spectrom.* **2014**, *28*, 483−488.
(60) Todd, A. R.; Barnes, L. F.; Young, K.; Zlotnick, A.; Jarrold, M. F. *Anal. Chem.* **2020**, *92*, 11357−11364.
(61) Skinner, O. S.; Haverland, N. A.; Fornelli, L.; Melani, R. D.; Do Vale, L. H. F.; Seckler, H. S.; Doubleday, P. F.; Schachner, L. F.; Srzentić, K.; Kelleher, N. L.; Compton, P. D. *Nat. Chem. Biol.* **2018**, *14*, 36−41.
(62) Mehaffey, M. R.; Xia, Q.; Brodbelt, J. S. *Anal. Chem.* **2020**, *92*, 15202−15211.
(63) Benesch, J. L. P.; Sobott, F.; Robinson, C. V. *Anal. Chem.* **2003**, *75*, 2208−2214.
(64) Herold, M.; Nierhaus, K. H. *J. Biol. Chem.* **1987**, *262*, 8826−8833.
(65) Hoffman, D. W.; Davies, C.; Gerchman, S. E.; Kycia, J. H.; Porter, S. J.; White, S. W.; Ramakrishnan, V. *EMBO J.* **1994**, *13*, 205−212.
(66) Hall, Z.; Hernández, H.; Marsh, J. A.; Teichmann, S. A.; Robinson, C. V. *Structure* **2013**, *21*, 1325−1337.
(67) Zhou, M.; Jones, C. M.; Wysocki, V. H. *Anal. Chem.* **2013**, *85*, 8262−8267.
(68) Gadkari, V. V.; Ramírez, C. R.; Vallejo, D. D.; Kurulugama, R. T.; Fjeldsted, J. C.; Ruotolo, B. T. *Anal. Chem.* **2020**, *92*, 15489−15496.

https://doi.org/10.1021/acs.analchem.1c00772
Anal. Chem. 2021, 93, 8484−8492

(69) Huguet, R.; Mullen, C.; Srzentić, K.; Greer, J. B.; Fellers, R. T.; Zabrouskov, V.; Syka, J. E. P.; Kelleher, N. L.; Fornelli, L. *Anal. Chem.* **2019**, *91*, 15732−15739.
(70) Bouchal, P.; Schubert, O. T.; Faktor, J.; Capkova, L.; Imrichova, H.; Zoufalova, K.; Paralova, V.; Hrstka, R.; Liu, Y.; Ebhardt, H. A.; Budinska, E.; Nenutil, R.; Aebersold, R. *Cell Rep.* **2019**, *28*, 832−843.
(71) Smith, L.; Agar, J.; Chamot-Rooke, J.; Danis, P.; Ge, Y.; Loo, J.; Pasa-Tolic, L.; Tsybin, Y.; Kelleher, N. *Preprints* **2020**, 2020100368.

https://doi.org/10.1021/acs.analchem.1c00772
Anal. Chem. 2021, 93, 8484−8492